Optimal Electromagnetic Searches for Axion and Hidden-Photon Dark Matter

Saptarshi Chaudhuri, ¹ Kent D. Irwin, ^{1,2,3} Peter W. Graham, ^{1,2,4} and Jeremy Mardon ¹ Department of Physics, Stanford University, Stanford, CA 94305 ² Kavli Institute for Particle Astrophysics and Cosmology, Stanford University, Stanford, CA 94305 ³ SLAC National Accelerator Laboratory, Menlo Park, CA 94025 ⁴ Stanford Institute for Theoretical Physics, Department of Physics, Stanford University, Stanford, CA 94305 (Dated: April 12, 2019)

Direct-detection searches for axions and hidden photons are playing an increasingly prominent role in the search for dark matter. In this work, we derive the properties of optimal electromagnetic searches for these candidates, subject to the Standard Quantum Limit (SQL) on amplification. We show that a single-pole resonant search may possess substantial sensitivity outside of the resonator bandwidth and that optimizing this sensitivity may increase scan rates by up to five orders of magnitude at low frequencies. Additional enhancements can be obtained with resonator quality factors exceeding one million, which corresponds to the linewidth of the dark matter signal. We present the resonator optimization in the broader context of determining the optimal receiver architecture (resonant or otherwise). We discuss prior probabilities on the dark matter signal and their role in the search optimization. We determine frequency-integrated sensitivity to be the figure of merit in a wideband search and demonstrate that it is limited by the Bode-Fano criterion. The optimized single-pole resonator is approximately 75% of the Bode-Fano limit, establishing it as a fundamentally near-ideal, single-moded dark matter detection scheme. Our analysis shows, in contrast to previous work, that the scanned single-pole resonant search is superior to a reactive broadband search. Our results motivate the broad application of quantum measurement techniques evading the SQL in future axion- and hidden-photon dark matter searches.

The existence of dark matter is one of the most compelling pieces of evidence for physics beyond the Standard Model.[1] Two of the leading candidates for darkmatter particles are weakly interacting massive particles (WIMPs) and axions. The axion is a pseudoscalar originally motivated as a solution to the strong CP problem [2]. Because of their low (usually sub-eV) mass, and therefore high number density if they make up a majority of the dark matter, axions are best described as classical fields oscillating at a frequency slightly higher than their rest frequency $\nu_{\rm DM}^0 = m_{\rm DM} c^2/h$, where $m_{\rm DM}$ is the rest mass. The observed frequency is slightly higher than the rest-mass frequency because of the $\sim 10^{-3}$ c virial velocity in the Milky Way; the resulting spread in kinetic energy gives axion dark matter a bandwidth of $\Delta\nu_{\rm DM}\sim 10^{-6}\nu_{\rm DM}^0$. The objective of axion searches is to detect this narrowband signal through its coupling to the Standard Model, either through the strong force [3] or electromagnetism [4, 5]. We focus on electromagnetic detection, in which an axion converts to a photon in a background DC magnetic field.

The hidden photon, a vector, is another well-motivated field-like dark-matter candidate that couples to electromagnetism (via kinetic mixing with the visible photon). It emerges generically in Standard Model extensions. [6–8] Additionally, hidden-photon dark matter may be produced by cosmic inflation. [9]

To date, most direct-detection searches for dark matter have focused on WIMPs.[10–12] For axions and hidden photons, a wide range of masses and couplings (the axion-photon coupling $g_{a\gamma\gamma}$ or the hidden photon mixing angle ε) have not been explored. Accordingly, numer-

ous searches looking for the conversion to photons have recently been proposed.[13, 14]

Because of the interest in these candidates, it is important to investigate the fundamental limits on the sensitivity of searches probing the electromagnetic coupling. A number of searches are based on tunable resonant structures.[15–22] When the resonant frequency is tuned to $\sim \nu_{\rm DM}^0$, the signal induced by dark matter rings up in the detector. One can conduct a sensitive search for dark matter by tuning the resonator across the desired search range. Are single-pole resonators optimal? Or can better sensitivity, integrated across a search band, be obtained with a more broadband structure, such as a broadband LR circuit [23] or a free-space antenna [24]?

The principal purpose of this paper is to determine the optimal characteristics of a dark matter receiver, subject to the Standard Quantum Limit (SQL) on phase-insensitive amplification.[25] The primary conclusion is that the optimized single-pole resonator is a fundamentally near-ideal, single-moded detector for probing dark matter across a wide band. We derive the optimized resonant scan, which exploits the substantial sensitivity available outside the resonator bandwidth. This optimization can increase scan rates by up to five orders of magnitude at low frequency. We further show that scan rate is enhanced by higher resonator quality factor, even for quality factors exceeding one million, which corresponds to the dark matter bandwidth. See [26] for an extended discussion of the results presented here.

In order to optimize the receiver and the scan, we take into account the signal-to-noise ratio (SNR) in the detection circuit as well as prior information about the dark matter signal. Priors can take the form of astrophysical or direct-detection constraints, preferred search ranges, or candidate signals. We optimize a value functional, which is the expectation value of the SNR squared (see eq. 107 of [26]):

$$F[H(\nu)] = E[SNR^2(H(\nu)); \nu_{DM}^0, g_{a\gamma\gamma}/\varepsilon, Q(\vec{v})], \quad (1)$$

where $H(\nu)$ is a responsivity function describing how dark matter at frequency ν excites the detector. The expectation value is taken with respect to user-defined prior probability distributions over the dark matter mass $m_{\rm DM}$ (corresponding to frequency $\nu_{\rm DM}^0$), coupling $g_{a\gamma\gamma}$ or ε , and velocity distribution $Q(\vec{v})$. The frequency ν lies within the dark matter bandwidth, slightly above $\nu_{\rm DM}^0$.

We first develop a circuit model to evaluate $H(\nu)$ and receiver SNR and then return to the subject of priors. The basic structure of a receiver is displayed in Fig. 1. The receiver is optimized by simultaneously optimizing each block and interactions across blocks, subject to priors. We restrict our attention to linear, passive receiver circuits.

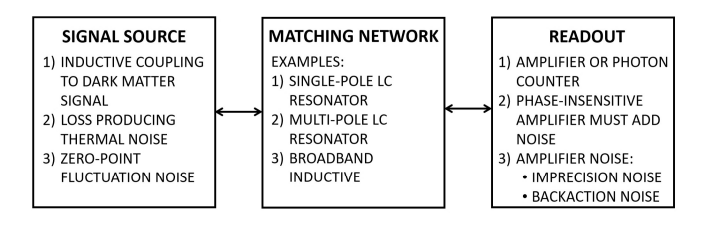


FIG. 1. Elements of a dark-matter receiver: the signal source, the matching network, and the readout. Double arrows signify that signals travel in both directions through the receiver.

The first element of the receiver is the signal source, which contains an element coupling to the electromagnetic fields induced by dark matter. The element may be reactive, e.g. an inductor coupling to the magnetic field or a capacitor coupling to the electric field. Alternatively, it may be purely resistive, e.g. a phased antenna array presenting a real impedance to the electric field signal.

In Sec. II of [26], we show that reactive coupling is superior to resistive coupling. In Sec. III of [26], we show that inductive coupling is optimal in the regime where the experimental apparatus is smaller than the dark-matter Compton wavelength $\lambda_{\rm DM}^0 = c/\nu_{\rm DM}^0$. In this regime, all couplings can be treated as reactive, and inductive coupling is always superior to capacitive coupling. When the apparatus is comparable in size to $\lambda_{\rm DM}^0$, inductive and capacitive couplings give comparable sensitivities. In the particular case of a cavity resonator, we can model the cavity as an equivalent lumped-element LC circuit. Then, coupling to the cavity mode through both the electric and magnetic fields can be modeled as an effective coupling to either the inductor or capacitor. Because of this equivalency, we may, without loss of generality, consider a model with only inductive coupling.

Intrinsic to every inductive coupling element L is some loss R, which produces thermal noise. We thus model the signal source as a series LR circuit.

The second element of the receiver is an impedance-matching network. It provides a match between the complex signal source impedance and the input impedance of the readout, which can be purely real. For example, the network may be a single-pole resonator (formed by inserting a capacitor), an appropriate model for cavity searches ADMX[15] and HAYSTAC[16] as well as lumped-element searches DM Radio[19, 20] and ADMX LC[21]. One may also consider using a multi-pole resonator. Yet another architecture is a broadband pickup circuit, for which the LR signal source is connected directly to the input of a SQUID amplifier, e.g. as used in ABRACADABRA.[23]

The third and final element of the receiver is a readout element, which is generically some amplifier or photon counter. In this work, we consider readout with a phase-insensitive amplifier, which amplifies both signal quadratures with equal gain. Such amplifiers are subject to the SQL [25, 27], which dictates that the measurement must add at least one photon of noise power per unit bandwidth. We utilize the convention that one-half photon of the quantum noise comes from zero-point fluctuations, while the other half comes from the amplifier's two effective noise modes, backaction and imprecision.[28]

We now consider how to calculate detector SNR. Probing new parameter space at a particular frequency typically requires integration time much longer than the coherence time $(\Delta \nu_{\rm DM})^{-1}$. In this regime, the signal to be detected is an incoherent power signal, for which the SNR is dictated by the Dicke radiometer equation[29, 30]:

$$SNR = \frac{P_{\text{sig}}}{P_{\text{noise}}} \sqrt{\Delta \nu_s \cdot t} = \frac{P_{\text{sig}}}{k T_S \Delta \nu_s} \sqrt{\Delta \nu_s \cdot t}, \quad (2)$$

where P_{sig} ($P_{\text{noise}} = kT_S\Delta\nu_s$) is signal (noise) power, T_S is system noise temperature (a function of the physical and amplifier noise temperatures), $\Delta\nu_s$ is effective dark-matter signal bandwidth when convolved with the responsivity function $H(\nu)$ (see Secs. IV and VI of [26]), and t is integration time. The system noise temperature is dependent upon the matching network, because the noise temperature of the amplifier depends on the impedance coupled to its input, achieving a minimum when the impedance is "noise matched." In order to fully optimize the third block (and the SNR), we must then simultaneously optimize the second block.

It is in the second block where priors play a central role. Most conceivable priors distribute the mass probability over a wide band. The value functional, eq. (1), is then a measure of a detector's frequency-integrated sensitivity. The significance of this observation can be understood by considering a single-pole resonator. See Fig. 2. The dark-matter signal and thermal noise are both rolled off by the resonator response. As such, the resonator sensitivity to dark matter (i.e. the SNR) remains constant

well beyond the resonator bandwidth, as long as amplifier noise is subdominant. For instance, the resonator sensitivity to the on-resonance dark matter signal ("DM 1"), is approximately equal to the sensitivity to a signal of equal strength off-resonance ("DM 2"). The "sensitivity bandwidth" is the range over which the amplifier noise is subdominant to thermal noise. This bandwidth can be increased by strengthening the coupling to the amplifier until amplifier backaction (not represented in figure), which degrades SNR, becomes comparable to the thermal noise. With a widely distributed mass prior, we must then choose the matching network not to maximize the on-resonance SNR, but to maximize a weighted product of sensitivity bandwidth and in-band SNR, i.e. integrated sensitivity. The sensitivity bandwidth increases with decreasing amplifier noise. Thus, for optimization, we require quantum-limited readout (achieving the SQL when noise-matched), even when the resonator, of frequency ν_r , possesses high thermal occupancy, $h\nu_r \ll kT$.

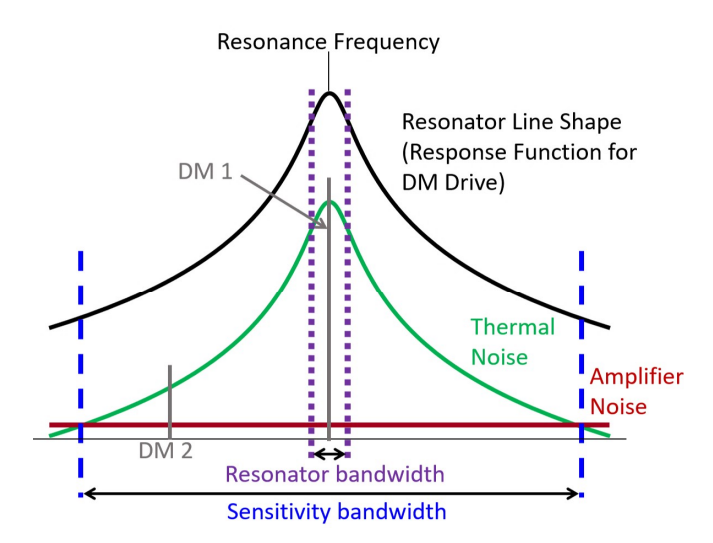


FIG. 2. Signal and noise in a resonator circuit. The x-axis is frequency detuning (arb. units, linear scale), while the y-axis is power referred to the amplifier input (arb. units, log scale). Green: thermal noise, red: amplifier noise, black: resonator line shape. On- and off-resonance dark matter (DM) signals of equal strength are denoted "DM 1" and "DM 2," respectively. The resonator bandwidth is bounded by the dotted purple lines, and the sensitivity bandwidth is bounded by dashed blue lines.

Frequency-integrated sensitivity as the figure of merit for a matching network (resonant or otherwise) is formalized mathematically in terms of priors in Sec. V of [26]. There we further develop a generic "log-uniform" search, characterized by a set of uninformative priors in which the probability distribution over mass is log-uniform. Fixing the LR source properties (the pickup inductance $L_{\rm PU}$, resistance R, and pickup volume) and

scaling out constants, eq. (1) reduces to (eq. 113 of [26])

$$F_{\log}[S_{21}(\nu)] = \int_{\nu_l}^{\nu_h} d\nu \left(\frac{|S_{21}(\nu)|^2}{|S_{21}(\nu)|^2 n(\nu) + 1} \right)^2, \quad (3)$$

where $S_{21}(\nu)$ is the forward transmission through the matching network and ν_l and ν_h are the lower and upper limits of the search range. $n(\nu)=1/(\exp(h\nu/kT)-1)$ is the thermal occupancy of the signal source at frequency ν . The "+1" term represents the noise at the SQL. The integrand thus represents SNR, and F_{\log} represents frequency-integrated sensitivity.

We maximize F_{log} . The signal source possesses complex impedance, and the quantum-limited amplifier possesses real noise impedance. If the matching network is linear, passive, and reciprocal, then the Bode-Fano criterion [31, 32] applies, yielding an upper bound on F_{log} (see Sec. V A 2 of [26]),

$$\frac{F_{\log}[S_{21}(\nu)]}{R/L_{\text{PU}}} \lessapprox \begin{cases} 0.4, & n(\nu_h) \ll 1\\ \frac{1}{4n(\nu_h)}, & n(\nu_h) \gg 1 \end{cases}$$
 (4)

The bound applies to an amplifier that measures forward power, as well as one that measures voltage or current (the "op-amp mode" [28]), e.g. a flux-to-voltage amplifier such as a SQUID; see App. F of [26]. An analogous bound applies to an RC (resistor and capacitor) source.

Equality in eq. (4) is obtained with a narrowband, multipole LC Chebyshev filter, but such structures are difficult to implement. Therefore, we ask how close a single-pole resonator can come to the Bode-Fano limit.

Suppose, having already fixed the LR source properties, we also fix the resonant frequency ν_r . The circuit is then determined by the strength of coupling to the amplifier, quantified by the ratio of noise impedance to signal source resistance. Optimizing eq. (3) with respect to this ratio, (Sec. V A 3 of [26])

$$\frac{F_{\log}^{\text{opt}}(\nu_r)}{R/L_{\text{PU}}} \approx \begin{cases} \frac{8}{27}, & n(\nu_r) \ll 1\\ \frac{1}{3\sqrt{3}n(\nu_r)}, & n(\nu_r) \gg 1 \end{cases}$$
(5)

Interestingly, we observe that, for optimal integrated sensitivity, the readout is noise-mismatched and dominated by backaction on resonance. To understand why, we consider readout with a quantum-limited flux-to-voltage amplifier (Fig. 3(a)) and the contributions to the inputreferred current noise for $n(\nu_r)=50$. In the noisematched case of Fig. 3(b), the amplifier noise on resonance is minimized, with equal backaction and imprecision. The result is a sensitivity bandwidth (given approximately by the bandwidth for which imprecision is less than one-half of the total noise[26]) that is $2\sqrt{n(\nu_r)}\approx 14$ resonator bandwidths. Now suppose that we couple more strongly to the amplifier, so that we achieve the optimal matching maximizing eq. (3). As illustrated in Fig. 3(c), the backaction noise increases to one-half of the thermal

noise on resonance, but the imprecision noise drops proportionally. In return for a 50% SNR penalty near resonance, we achieve a much larger sensitivity bandwidth of $2n(\nu_r)\sqrt{3}\approx 173$ resonator bandwidths, yielding a larger integrated sensitivity in eq. (3).

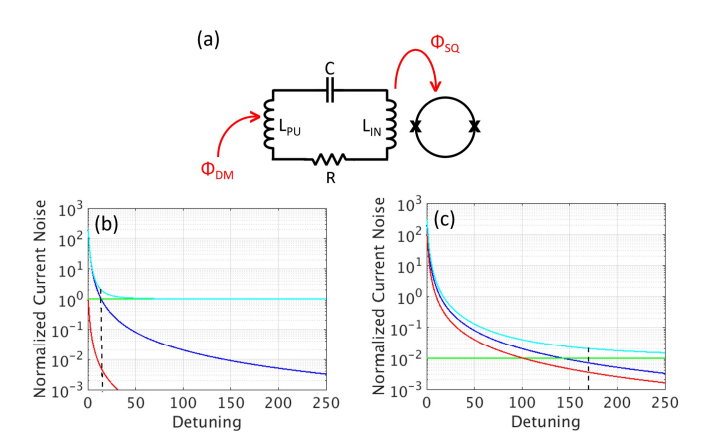


FIG. 3. (a) RLC search. The flux Φ_{DM} couples to the pickup inductor, driving a flux Φ_{SQ} in the amplifier, shown schematically as a dc SQUID. We plot detuning $2Q\frac{\nu-\nu_r}{\nu_r}$ vs. input-referred current noise spectral density $S_{II}/(h\nu_r/R)$ in the (b) noise-matched and (c) optimally-matched circuits for $n(\nu_r)=50$. Blue: thermal + zero-point noise, green: imprecision, red: backaction, cyan: total noise. Detunings below the dashed black line are in the sensitivity bandwidth.

 $F_{\log}^{\mathrm{opt}}(\nu_r)$ is an increasing function of ν_r , so an appropriate comparison to the Bode-Fano limit (eq. 4) is obtained by taking the limit $\nu_r \to \nu_h$. We then find (eq. 146 of [26]) that the optimized single-pole resonator is approximately 75% of the Bode-Fano limit. Single-pole resonators are near-optimal, single-moded detectors for a search over a wide band. One consequence of this result is that, in contrast to the claims in [23], a tunable RLC circuit is superior to a broadband LR circuit, e.g. as used in ABRACADABRA; see App. G of [26] for details.

We now return to a consideration of priors and discuss scanning. An optimal search requires scanning for complete coverage of a search band. Given a fixed total experiment time, what value function do we use to distribute time across scan steps? A scan consists of a set of resonant frequencies $\{\nu_r^i\}$; at each frequency, we integrate for time τ_i . For axion searches, the time allocation is optimized by maximizing the weighted area of the excluded mass-coupling parameter space:

$$A_a[\{\nu_r^i\}, \{\tau_i\}] = \int_{\nu_l}^{\nu_h} d\nu_{\rm DM}^0 \int_{g_{a\gamma\gamma}^{\rm min}}^{g_{a\gamma\gamma}^{\rm max}} dg_{a\gamma\gamma} W_a.$$
 (6)

 $W_a = W_a(\nu_{\rm DM}^0, g_{a\gamma\gamma})$ is the weighting function, based on mass and coupling priors introduced for eq. (1). $g_{a\gamma\gamma}^{\rm min} = g_{a\gamma\gamma}^{\rm min}(\nu_{\rm DM}^0, \{\nu_r^i\}, \{\tau_i\})$ is the minimal coupling at $\nu_{\rm DM}^0$ to which the search is sensitive, based on the SNR accrued from integration at each scan step. $g_{a\gamma\gamma}^{\rm max} = g_{a\gamma\gamma}^{\rm max}(\nu_{\rm DM}^0)$ is

a maximal coupling, based on previous constraints. An analogous value function, using ε , can be defined for the hidden photon. For a log-uniform search, in which W_a is proportional to the product of log-uniform distributions over mass and coupling, maximizing eq. (6) shows that equal time should be spent in each octave of frequency space; see Sec. V B of [26].

Our scan optimization also reveals that the SNR improves as the quality factor is increased above $Q_{\rm DM} =$ 10⁶, the characteristic quality factor of the dark matter signal. To explain this result, we return to eq. (2) and assume $\nu_{\rm DM}^0$ lies near resonance. In a single scan step with $Q > Q_{\rm DM}$, the signal power is roughly independent of Q because an increase in Q is compensated by a reduction in signal fraction within the resonator bandwidth. The noise power decreases as 1/Q because $\Delta \nu_s$ equals the resonator bandwidth. The integration time also decreases as 1/Q because more scan steps are required with a finer bandwidth. Combining all factors, the SNR from the single step is roughly independent of Q. Stepping at one part in $\sim Q$, we are sensitive to the same mass over $\sim Q/Q_{\rm DM}$ scan steps. The SNRs from different steps add in quadrature so the total SNR improves as $\sim \sqrt{Q}$.

In Fig. 4, we plot scan sensitivity to axion-photon coupling. A resonator can probe all frequencies within its sensitivity bandwidth without SNR degradation. Thus, relative to a noise-matched scan using only information in the resonator bandwidth (dark blue with $Q = 10^6$), a scan with optimized integrated sensitivity (light blue with $Q = 10^6$) increases the integration time at frequency $\nu_{\rm DM}^0$ by $\sim n(\nu_{\rm DM}^0)$. Then, from eq. (2), since signal power increases as coupling squared[5], the minimum coupling to which the search is sensitive improves by $\sim n(\nu_{\rm DM}^0)^{1/4}$. This corresponds to more than an order of magnitude increase in reach at ~ 1 kHz, or equivalently, a five order of magnitude increase in scan rate. Additionally, sensitivity outside of the resonator bandwidth increases the step size needed for complete coverage of a search band, enabling significantly coarser tuning. By increasing Q to 10⁸ (pink), we further enhance the reach by a factor of $\sqrt{10}$ (100× increase in scan rate).

In summary, we have established the fundamental limit on electromagnetic searches for axion and hidden-photon dark matter including the quantum noise from amplifiers (eq. 4). We have demonstrated that the single-pole resonator is a near-ideal single-moded technique for dark matter searches over a wide band, justifying the approach of multiple experiments [15, 16, 19, 21]. We have shown that optimal scan strategies can increase the scan rate by several orders of magnitude, particularly at low mass.

Fig. 4 demonstrates that, given practical constraints on experimental volume, temperature, loss, DC magnetic field, and integration time, no electromagnetic receiver subject to the limits established in this paper may probe the QCD axion band at frequencies $\lesssim 1$ MHz, corresponding to masses below a few neV. Similar

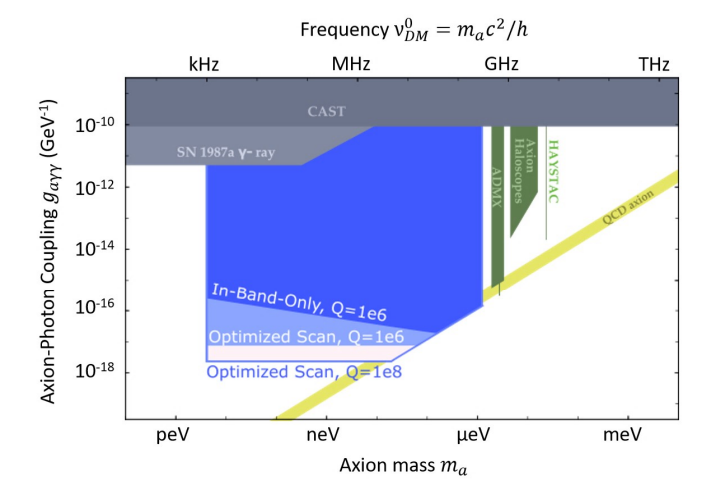


FIG. 4. Axion search with quantum-limited readout, 1 m^3 volume at 10 mK, 4 T magnetic field, and up to 100 days per e-folding integration time (stopped at the DFSZ axion model) over 1 kHz-300 MHz. Sensitivity (eq. 197 of [26]) for: a $Q=10^6$ scan using only information in the resonator bandwidth (dark blue), an optimized $Q=10^6$ scan (light blue), and an optimized $Q=10^8$ scan (pink). We have assumed a geometry factor of $c_{\rm PU}\approx 0.2$, which is reasonable for lumped-element receivers [19, 20]; see Appendix A of [26]. The QCD axion band (yellow) is bounded at the top and bottom by the KSVZ[33, 34] and DFSZ[35, 36] axion models, respectively.

challenges exist above several GHz. As such, it is useful to ask how we may evade the limits established in this work. One may evade the Bode-Fano constraint, for instance, by using nonlinear or active impedance-matching circuits; one may also improve upon the constraint using multi-moded receivers, or more generically, receivers with multiple signal-source ports. These circuits are often constrained by more generalized matching criteria [37, 38] and can be challenging to implement due to stability and parasitics. The other option is to improve on these limits by evading the SQL. Due to developments in quantum metrology, a number of techniques to evade the SQL (e.g. squeezing, entanglement, backaction evasion, photon counting) can now be deployed. [39] The fundamental limit provided in this paper thus motivates the development of quantum measurement techniques in light-field dark matter searches.

This research is funded by the Heising-Simons Foundation, the Moore Foundation, SLAC Laboratory Directed Research and Development, the Kavli Institute for Particle Astrophysics and Cosmology, and DOE HEP QuantISED award #100495. We thank Asimina Arvanitaki, Hsiao-Mei Cho, Carl Dawson, Michel Devoret, Stephen Kuenstner, Konrad Lehnert, Dale Li, Harvey Moseley, Lyman Page, Arran Phipps, Surjeet Rajendran, Jamie Titus, Tony Tyson, Betty Young, and Jonas Zmuidzinas for useful discussions.

- [1] P. A. Ade, N. Aghanim, M. Alves, C. Armitage-Caplan, M. Arnaud, M. Ashdown, F. Atrio-Barandela, J. Aumont, H. Aussel, C. Baccigalupi, et al., Astronomy & Astrophysics 571, A1 (2014).
- R. Peccei and H. Quinn, Phys. Rev. Lett. 38, 1440 (1977).
- [3] D. Budker *et al.*, Phys. Rev. $\mathbf{X4}$, 021030 (2014), arXiv:1306.6089 [hep-ph].
- [4] P. Sikivie, Phys. Rev. Lett. **51**, 1415 (1983).
- [5] P. Sikivie, Phys. Rev. D 32, 2988 (1985).
- [6] B. Holdom, Physics Letters B 178, 65 (1986).
- [7] A. Nelson and J. Scholtz, Phys. Rev. **D84**, 103501 (2011), arXiv:1105.2812 [hep-ph].
- [8] P. Arias, D. Cadamuro, M. Goodsell, J. Jaeckel, J. Redondo, and A. Ringwald, JCAP 2012, 013 (2012).
- [9] P. Graham, J. Mardon, and S. Rajendran, Phys. Rev. D93, 103520 (2016), arXiv:1504.02102 [hep-ph].
- [10] R. Agnese et al. (SuperCDMS), Phys. Rev. Lett. 116, 071301 (2016).
- [11] D. Akerib et al. (LUX Collaboration), Phys. Rev. Lett. 118, 021303 (2017).
- [12] E. Aprile, M. Alfonsi, K. Arisaka, F. Arneodo, C. Balan, L. Baudis, B. Bauermeister, A. Behrens, P. Beltrame, K. Bokeloh, et al., Phys. Rev. Lett. 109, 181301 (2012).
- [13] P. W. Graham, I. G. Irastorza, S. K. Lamoreaux, A. Lindner, and K. A. van Bibber, Annual Review of Nuclear and Particle Science 65, 485 (2015).
- [14] I. G. Irastorza and J. Redondo, Progress in Particle and Nuclear Physics (2018).
- [15] N. Du, N. Force, R. Khatiwada, E. Lentz, R. Ottens, L. Rosenberg, G. Rybka, G. Carosi, N. Woollett, D. Bowring, et al., Physical review letters 120, 151301 (2018).
- [16] B. Brubaker, L. Zhong, Y. Gurevich, S. Cahn, S. Lamoreaux, M. Simanovskaia, J. Root, S. Lewis, S. Al Kenany, K. Backes, et al., Physical review letters 118, 061302 (2017).
- [17] L. Zhong, S. Al Kenany, K. Backes, B. Brubaker, S. Cahn, G. Carosi, Y. Gurevich, W. Kindel, S. Lamoreaux, K. Lehnert, et al., Physical Review D 97, 092001 (2018).
- [18] B. Brubaker, L. Zhong, S. Lamoreaux, K. Lehnert, and K. van Bibber, Physical Review D 96, 123008 (2017).
- [19] S. Chaudhuri et al., Phys. Rev. **D92**, 075012 (2015), arXiv:1411.7382 [hep-ph].
- [20] M. Silva-Feaver et al., IEEE Transactions on Applied Superconductivity 27, 1 (2017).
- [21] P. Sikivie, N. Sullivan, and D. Tanner, Phys. Rev. Lett. 112, 131301 (2014).
- [22] A. Caldwell, G. Dvali, B. Majorovits, A. Millar, G. Raffelt, J. Redondo, O. Reimann, F. Simon, F. Steffen, M. W. Group, et al., Physical Review Letters 118, 091801 (2017).
- [23] Y. Kahn *et al.*, Physical Review Letters **117**, 141801 (2016).
- [24] D. Horns, J. Jaeckel, A. Lindner, J. Redondo, A. Ringwald, et al., Journal of Cosmology and Astroparticle Physics 2013, 016 (2013).
- [25] C. M. Caves, Phys. Rev. D 26, 1817 (1982).
- [26] S. Chaudhuri, K. Irwin, P. W. Graham, and J. Mardon, arXiv preprint arXiv:1803.01627 (2018).
- [27] A. Clerk, Physical Review B **70**, 245306 (2004).

- [28] A. A. Clerk, M. H. Devoret, S. M. Girvin, F. Marquardt, and R. J. Schoelkopf, Rev. Mod. Phys. 82, 1155 (2010).
- [29] R. H. Dicke, Review of Scientific Instruments 17, 268 (1946).
- [30] S. Asztalos *et al.*, Physical Review Letters **104**, 041301 (2010).
- [31] H. W. Bode, Network analysis and feedback amplifier design (van Nostrand, 1945).
- [32] R. M. Fano, Journal of the Franklin Institute **249**, 57 (1950).
- [33] M. A. Shifman, A. Vainshtein, and V. I. Zakharov, Nuclear Physics B 166, 493 (1980).

- [34] J. E. Kim, Physical Review Letters 43, 103 (1979).
- [35] M. Dine, W. Fischler, and M. Srednicki, Physics letters B 104, 199 (1981).
- [36] A. Zhitnitskij, Yadernaya Fizika **31**, 497 (1980).
- [37] D. Youla, IEEE Transactions on Circuit Theory 11, 30 (1964).
- [38] D. Nie and B. M. Hochwald, IEEE Transactions on Circuits and Systems I: Regular Papers 62, 995 (2015).
- [39] H. Zheng, M. Silveri, R. Brierley, S. Girvin, and K. Lehnert, arXiv preprint arXiv:1607.02529 (2016), arXiv:1607.02529v2 [hep-ph].